Materials Research. 2025; 28(suppl. 1): e20240583
DOI: https://doi.org/10.1590/1980-5373-MR-2024-0583

Modified *Moringa oleifera* Seed Husk Biomass as an Eco-Friendly Adsorbent for Emerging Contaminant Bisphenol A Removal from Water

Cely Roledo*[a,b], *Victória Agnes Salgueiro Ferreira*[a], *Kleper de Oliveira Rocha*[c], *Adriano Gonçalves dos Reis*[a]

[a]*Universidade Estadual Paulista (UNESP), Instituto de Ciência e Tecnologia, Departamento de Engenharia Ambiental, São José dos Campos, SP, Brasil.*
[b]*Companhia Ambiental do Estado de São Paulo (CETESB), São Paulo, SP, Brasil.*
[c]*Universidade Estadual Paulista (UNESP), Faculdade de Ciências, Departamento de Química, Bauru, SP, Brasil.*

Received: December 12, 2024; Revised: March 17, 2025; Accepted: May 17, 2025

Bisphenol A (BPA), commonly found in plastics and epoxy resins, poses serious risks to human and animal health, particularly affecting reproduction and hormonal balance. This study investigates the removal of BPA from water using modified *Moringa oleifera* seed husks (H-MOH300) as a sustainable adsorbent. The husks were chemically activated with phosphoric acid and thermally treated at 300°C, yielding a BET surface area of 380 $m^2\ g^{-1}$ and a pore volume of 0.282 $cm^3\ g^{-1}$. SEM analysis showed a porous and fibrous morphology, while XRD indicated a crystalline nature. FTIR identified hydroxyl, aromatic, and carboxylic functional groups. The process followed the Langmuir isotherm model, achieving a maximum adsorption capacity of 27.5 mg g^{-1} at 22°C. Thermodynamic analysis indicated a spontaneous, endothermic process driven by electrostatic and π-π interactions. Regeneration tests up to 5 cycles confirmed H-MOH300's reusability, demonstrating its potential as a cost-effective, eco-friendly solution for BPA removal.

Keywords: *Adsorption, BPA, Contaminants of emerging concern, Endocrine disruptor, Low-cost adsorbent.*

Visual abstract

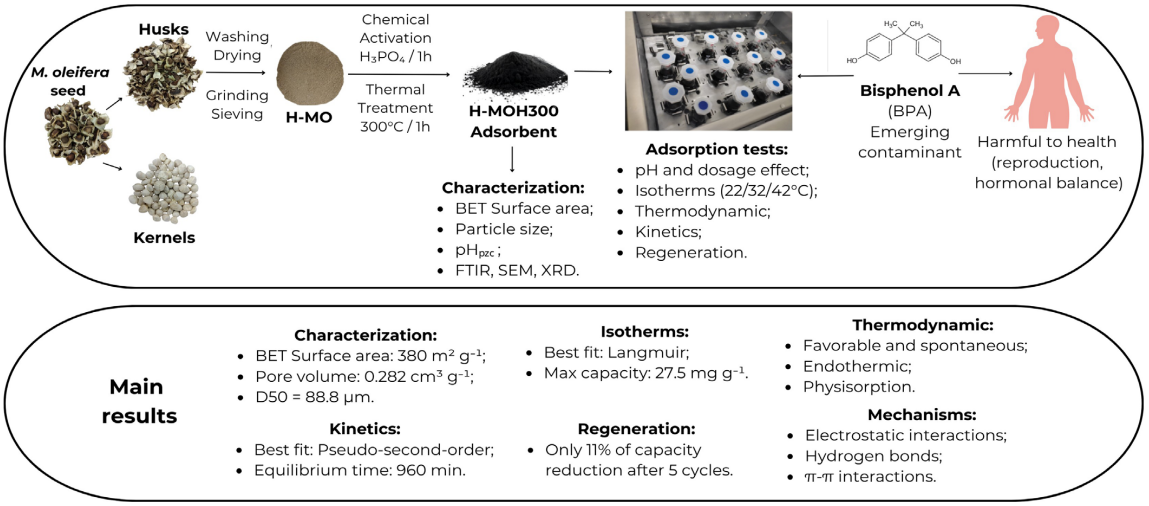

*e-mail: adriano.reis@unesp.br
Associate Editor: Leonardo Gondim de Andrade e Silva
Editor-in-Chief: Luiz Antonio Pessan

1. Introduction

The substance 2,2-bis(4-hydroxyphenyl) propane, commonly known as bisphenol A (BPA), is frequently used to produce epoxy resins and polycarbonate plastics. BPA is also used in the industrial manufacturing of plastic bottles, can linings, and thermal papers[1]. Many studies have highlighted the harmful effects of BPA, including its impact on reproduction, genetics, the nervous system, embryo development, and hormonal balance[2,3]. The permissible BPA concentration differs depending on the water source. Regulating BPA levels within the 1–15 μg L^{-1} range in freshwater, seawater, and wastewater is essential to protecting aquatic ecosystems[4]. Studies have shown worldwide BPA contamination in freshwaters used as sources of drinking water after treatment, especially in the most industrialized and urbanized regions[5-9]. Considering that the conventional drinking water treatment process, which involves coagulation, flocculation, sedimentation, and filtration stages, has low BPA removal rates[10,11] and is the most applied process worldwide[12], developing alternative treatments for BPA removal from water is imperative.

Various methods for removing BPA from water, including membrane filtration, biological processes, ultraviolet (UV) irradiation, and advanced oxidation techniques, have been investigated. The main advantage of these methods is their high capacity commonly found for removing BPA from water. However, challenges such as high cost and energy consumption, the generation of toxic by-products, and the use of hazardous chemicals limit the widespread implementation of these technologies on a large scale[13,14].

Adsorption is also considered an effective method for BPA removal[15,16] and offers multiple benefits, such as simplicity, cost-effectiveness, high efficiency, and the absence of hazardous byproduct formation[17]. However, large-scale application of commercial activated carbons is still a challenge because of their high costs for activation related to energy consumption (500–900 °C)[14]. To address these challenges, increasing attention has been given to developing and producing environmentally friendly adsorbents using low-cost agricultural waste materials.

The utilization of agricultural waste materials as adsorbents to eliminate BPA has garnered significant attention. This is due to their abundance in nature, diverse functional groups, eco-friendliness, low cost, ease of surface modification, chemical stability, renewability, and biodegradability. These qualities make them favourable for regeneration and reuse after adsorption[14,18]. Therefore, developing new low-cost and eco-friendly adsorbents to remove BPA from water is essential.

Moringa oleifera (MO) is a plant belonging to the *Moringaceae* family that is native to India and the sub-Himalayan regions. MO is now commonly found in tropical areas, including the American continent[19]. In addition to the various applications of MO as a food and medicinal plant, MO seeds have been used as a natural coagulant in water and wastewater treatment[20-22]. However, the use of MO seeds generates husks as waste, which have been studied for potential applications as adsorbents for different contaminants, such as methylene blue[23], atrazine[24], and acetaminophen[25]. The probable explanation for the promising adsorption results lies in the structure, micropore volume, and composition of the materials, as adsorption is favored by the presence of carboxyl, hydroxyl, and carbonyl groups[26]. However, no studies in the literature have reported the potential use of MO seed husks as an adsorbent for bisphenol A (BPA) removal. Furthermore, research using MO husks as adsorbents indicates a low surface area post-activation, with surface areas such as 10.32 m^2 g^{-1} [24] and 4.6 m^2 g^{-1} [25]. Further studies are needed to enhance this crucial property for effective adsorption.

In this context, given the urgent need for low-cost and eco-friendly adsorbents to remove BPA from water due to its risks to human health and the environment, as well as the necessity to repurpose *Moringa oleifera* seed husk residues, this study introduces a novel approach by optimizing the activation method for MO seed husks and demonstrating their effectiveness as a sustainable adsorbent for BPA removal. This research provides a comprehensive investigation, including advanced adsorbent characterization using scanning electron microscopy (SEM), X-ray diffraction (XRD), Brunauer-Emmett-Teller (BET) surface area analysis, Fourier transform infrared (FTIR) spectroscopy, particle size distribution, and point of zero charge determination. Various kinetic and isotherm models were assessed to elucidate the adsorption mechanism and thermodynamic behavior. Furthermore, the adsorbent's performance was critically evaluated against previous studies using different adsorbents for BPA removal, and its regeneration capacity was tested, reinforcing its potential as an efficient and reusable material for water decontamination.

2. Materials and Methods

2.1. Chemicals and Reagents

Moringa oleifera seeds were purchased from Arbocenter, Brazil and the BPA (purity ≥ 99%) was procured from Sigma-Aldrich. In chemical activation processes, potassium hydroxide (KOH) (purity ≥ 85%, ACS Científica) or phosphoric acid (H_3PO_4) (purity 85%, Vetec) was used. The point of zero charge (pH_{PZC}) test used the reagent $NaNO_3$ (purity ≥ 98%, Êxodo Científica) and for pH adjustments was used HCl (purity = 36.80%, Neon) or NaOH (purity = 98.81%, Neon).

2.2. Adsorbent Preparation

Moringa oleifera seeds were manually peeled, and the seed husks were dried at 105°C for 2 h. After drying, the husks were ground and sifted to be standardized to a 28-mesh (600 μm) maximum particle size. The obtained powder was used as an adsorbent (H-MO) and was also the precursor for the chemically and thermally treated adsorbents.

Chemical activation (CA) was carried out via potassium hydroxide (KOH) or phosphoric acid (H_3PO_4), as these reagents have shown promising results in activating precursors from agricultural waste to remove BPA[16,27,28]. CA occurred at a mass ratio of 1:5 m/v (H-MO/KOH or H_3PO_4) in aqueous solution (0.1 mol L^{-1}), which was maintained for 1 h at room temperature and then dried at 105°C for 15 h. The chemically activated material was subsequently thermally activated in a single stage (carbonization and activation) in a muffle furnace (LF02310, Jung) at a heating rate of 20°C min^{-1} under two different conditions (300°C or 500°C) for 1 h. The mixture

was then washed with deionized water until a neutral pH was reached. Only thermal activation of H-MO at 750°C for 30 min (H-MO750) was also carried out. A summary of the chemical and physical activations is presented in Table 1 and a schematic diagram describing the fabrication process of the adsorbents is presented in Figure 1. After preliminary adsorption tests, the most promising material was chosen for the study.

2.3. Characterisation

The adsorbent was characterized by scanning electron microscopy (SEM) (FEI model INSPECT S50 equipment) to determine the surface morphology, N_2 physisorption (BET) (NOVA 4200e, Quantachrom) to determine the specific surface area, Fourier transform infrared spectroscopy (FTIR) (IR PRESTIGE-21, Shimadzu) operating in the attenuated total reflectance (ATR) mode to determine the surface functional groups, multi-laser technology to determine the particle size distribution (CILAS 1190, CPS US, Inc.), and X-ray diffraction analysis (XRD) (Miniflex 600, Rigaku) to evaluate the structural properties. The crystallinity index (CI) was calculated through the deconvolution of the peaks from XRD using OriginPro® 2024, as presented in Equation 1[29].

$$CI(\%) = \frac{A_p}{A_t} \times 100 \quad (1)$$

where A_p is the integrated area of the peak and A_t is the total integrated area.

The point of zero charge (pH_{PZC}) test was performed via the salt addition method with $NaNO_3$ in an aqueous solution (0.1 mol L^{-1}) according to Bakatula et al.[30]. In the '11 point experiment' method, 50 mL of $NaNO_3$ solution at different initial pH values (2.0, 3.0, 4.0, 5.0, 6.0, 7.0, 8.0, 9.0, 10.0, 11.0 and 12.0) adjusted with HCl (0.1 mol L^{-1}) or NaOH (0.1 mol L^{-1}) was added to 0.2 g of sample, which was shaken on a temperature-controlled stirring apparatus (Dubnoff 304-TPA) at 100 rpm and 22°C for 16 h.

Table 1. Chemical and physical activations using *M. oleifera* seed husk powder as a precursor.

Adsorbent	Chemical activation	Physical activation
H-MO	-	-
H-MO750	-	750°C/30 min
H-MOK300	KOH/60 min	300°C/60 min
H-MOK500	KOH/60 min	500°C/60 min
H-MOH300	H_3PO_4/60 min	300°C/60 min

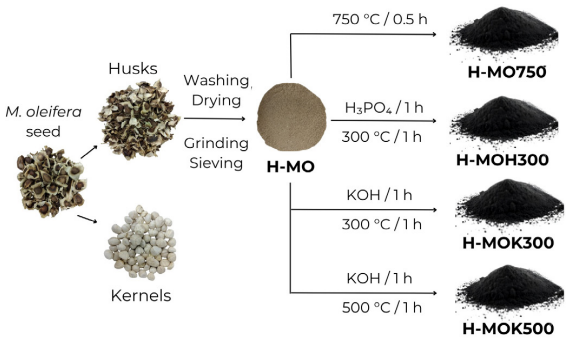

Figure 1. Schematic diagram describing the fabrication process of the adsorbents.

2.4. Adsorption studies

Preliminary adsorption tests were conducted with the adsorbents H-MO, H-MO 750, H-MOK300, H-MOK500, and H-MOH300 in the batch adsorption process using a 2 g L^{-1} dosage of the adsorbent in 50 mL of BPA solution with a 20 mg L^{-1} concentration for 24 h at room temperature to evaluate the most promising candidate for BPA removal. As the literature shows that BPA can be quantified using a spectrophotometric method at wavelengths between 270 and 290 nm [31-33], the developed quantification method was performed with a UV–Vis spectrophotometer (Genesys 50, Thermo Fisher Scientific) at 276 nm.

The adsorption tests were carried out in batch mode in triplicate via a temperature-controlled stirring apparatus (Dubnoff 304-TPA) at 100 rpm at room temperature for 24 h. The adsorbent dosage effect was evaluated using 0.6, 1.0, 1.6, 2.0, 3.0, 4.0, 5.0, and 6.0 g L^{-1} adsorbent in 50 mL of BPA (20 mg L^{-1}) at a pH of 6.0. To evaluate the effect of the pH, 2.0 g L^{-1} adsorbent and 50 mL of BPA (20 mg L^{-1}) solution were used, and the pH was adjusted to 5.0, 6.0, 7.0, 8.0, 9.0, 10.0, 11.0, 12.0, and 13.0.

2.5. Adsorption kinetics

The kinetic study was conducted under the optimal conditions, with 2.0 g L^{-1} adsorbent in 50 mL of BPA solution (20 mg L^{-1}). The contact time intervals from the analysed samples were 0.5–32 h at a temperature of 22°C at 100 rpm. After the contact time, the solutions were filtered through a Whatman Grade 1 filter, and the BPA concentration was quantified. The data were subjected to nonlinear regression analysis via the OriginPro® 2024 software program. The adsorption capacity q (mg g^{-1}) was calculated, as presented in Equation 2[34].

$$q = \frac{(C_o - C_e)\,V}{m} \quad (2)$$

where C_0 and C_e are the initial and equilibrium concentrations of BPA, respectively (mg L^{-1}), V is the volume of BPA solution (L), and m is the adsorbent mass (g).

Kinetic studies were conducted via the pseudo-first-order (PFO) equation proposed by Lagergren[35], the pseudo-second-order (PSO) equation proposed by Ho and Mckay[36], the intraparticle diffusion equation proposed by Weber and Morris[37], and the Elovich equation proposed by McLintock[38]. These kinetic equations are expressed as Equations 3, 4, 5 and 6, respectively.

$$q_t = q_e\left[1 - e^{-k_1 t}\right] \quad (3)$$

where q_t and q_e are the adsorption capacities at time t and at equilibrium (mg g^{-1}), t is the contact time (min), and k_1 is the pseudo-first-order rate constant (min^{-1}).

$$q_t = \frac{k_2 q_e^2 t}{1 + k_2 q_e t} \quad (4)$$

where q_t and q_e are the adsorption capacities at time t and at equilibrium (mg g^{-1}), t is the contact time (min), and k_2 is the pseudo-second-order rate constant (g mg^{-1} min^{-1}).

$$q_t = K_{dif}\sqrt{t} + C \quad (5)$$

where K_{dif} is the intraparticle diffusion rate constant (mg g^{-1} $min^{1/2}$), q_t is the adsorption capacity at time t (mg g^{-1}), t is the adsorption time (min), and C is the constant related to the thickness of the boundary layer (mg g^{-1}).

$$q_t = \frac{1}{\beta}\ln(1+\alpha\beta t) \quad (6)$$

where q_t is the adsorption capacity at time t (min), α is the initial rate constant (mg g^{-1} mg^{-1}), and β is the desorption constant during experiment (mg g^{-1}).

2.6. Adsorption isotherms

Three different temperatures (22°C, 32°C, and 42°C) were used to determine the adsorption equilibrium of BPA and the effect of temperature. A BPA concentration of 10–120 mg L^{-1} was studied in 50 mL of solution, with 2.0 g L^{-1} adsorbent, a contact time of 16 h, a pH of 6.0, and a stirring speed of 100 rpm. After the conclusion of the contact time, the BPA concentration was analysed.

This study tested the Langmuir, Freundlich, and Temkin isotherm models via nonlinear regression analysis. The Langmuir isotherm assumes a finite number of independent active sites, with no interaction or competition between them. The adsorption probability at an active site remains unaffected by the occupation of neighbouring sites. The Langmuir equation is presented in Equation 7[39].

$$q_e = \frac{q_{máx}\, k_L\, C_e}{1 + k_L\, C_e} \quad (7)$$

where k_L is the isothermal constant of Langmuir (L mg^{-1}) and q_{max} is the maximum adsorption capacity (mg g^{-1}).

The Freundlich model is related to heterogeneous surfaces and does not make assumptions about the adsorption capacity of the monolayer. Instead, it assumes that adsorbed molecules interact. It is presented in Equation 8[40].

$$q_e = K_F C_e^{1/n} \quad (8)$$

where, K_F is Freundlich's isothermal constant (mg L^{-1}) (L $g^{-1})^{1/n}$ and 1/n is the Freundlich intensity parameter.

The Temkin and Pyzhev model assumes that the process heat decreases linearly as the surface layers of the solid increase[41], as presented in Equation 9.

$$q_e = \frac{RT}{b_T}\ln(K_T C_e) \quad (9)$$

where, b_T is the Temkin constant related to adsorption heat (J mol^{-1}), K_T is the isothermal equilibrium constant related to the maximum binding energy (L mg^{-1}), R is the universal gas constant (8.314 J mol^{-1} K^{-1}) and T is the temperature of the solution (K).

2.7. Thermodynamics

Thermodynamic studies are indispensable for understanding adsorption mechanisms[42]. Based on the equilibrium adsorption experimental data, the thermodynamic parameters can be calculated according to thermodynamic laws. The Gibbs free energy (ΔG°) (kJ mol^{-1}) was estimated according to Equation 10[43].

$$\Delta G° = -RT\ln K_C \quad (10)$$

The relationships among ΔG°, enthalpy (ΔH°) (kJ mol^{-1}) and entropy (ΔS°) (J mol^{-1} K^{-1}) are described in Equation 11, and the van't Hoff Equation 12 is obtained by substituting Equation 10 into Equation 11[43].

$$\Delta G° = \Delta H° - T\Delta S° \quad (11)$$

$$\ln K_C = -\frac{\Delta H°}{R}\frac{1}{T} + \frac{\Delta S°}{R} \quad (12)$$

where R is the ideal gas constant (8.314 J mol^{-1} K^{-1}) and T is the temperature in K.

K_C should be dimensionless and was obtained by multiplying K_L by the molecular weight of the adsorbate (M_W) (g mol^{-1}), by 1,000, and then by 55.5 [Equation 13][44].

$$K_C = M_W\, x 55.5\, x 1{,}000\, x\, K_L \quad (13)$$

2.8. Regeneration study

To investigate the reusability of the adsorbent, an adsorption test was carried out with 250 mL of BPA solution (120 mg L^{-1}) and 2.0 g L^{-1} adsorbent at 22°C for 16 h. The loaded adsorbent was filtered and washed thoroughly with deionized water. It was then introduced into 50 mL of ethanol solution (75% v/v) (purity 95.1–96.9%, Merck) and stirred at 100 rpm for 5 h. Ethanol was chosen because it was shown to be a proper substance for BPA desorption from other adsorbents[18,19,45]. The regenerated adsorbent was filtered, washed thoroughly with deionized water, and dried at 105°C for 1 h. Five adsorption–desorption cycles were carried out in triplicate, and the adsorption capacity q (mg g^{-1}) was measured after each cycle.

3. Results and Discussion

3.1. Activation performance

The five types of adsorbents produced were preliminarily tested in the batch adsorption process. The efficiency of BPA removal in preliminary tests and the yield rate were calculated and are shown in Table 2. The H-MOH300 adsorbent was selected for this study based on its ability to remove BPA from aqueous solution (67% removal and an adsorption capacity of 6.6 mg g^{-1}) and its production yield (26%) compared with those of the other adsorbents studied.

Table 2. Adsorption of BPA by different adsorbents derived from H-MO with different chemical and thermal activations.

Adsorbent	q (mg g^{-1})	BPA Removal %	Yield rate %
H-MO	0	0	83.9
H-MO750	0	0	1.5
H-MOK300	0	0	10.8
H-MOK500	2.3	15.5	2.1
H-MOH300	6.6	66.6	25.6

3.2. Characterization

3.2.1. BET analysis and particle size distribution

The N_2 adsorption–desorption curves of the H-MOH300 adsorbent are presented in Figure 2, which shows the behaviour of a reversible type II isotherm. This type of isotherm is typical of a macroporous material with gradual curvature related to monolayer coverage (point B), indicating multilayer adsorption[44]. The hysteresis loop is type H3, which is characteristic of nonrigid aggregates of plate-like particles, despite desorption not converging to adsorption. The curves for adsorption/desorption do not overlap, possibly because N_2 might have been trapped between the plates or fibres, and at P/P_0 values below 0.5, the cavitation process forced out N_2.

H-MOH300 presented a BET specific surface area and total pore volume of 380 $m^2\ g^{-1}$ and 0.282 $cm^3\ g^{-1}$, respectively. Compared with those of H-MO, the specific surface area and porosity of H-MO increased after chemical and thermal treatment, which presented a surface area and total pore volume of 3.24 $m^2\ g^{-1}$ and 0.010 $cm^3\ g^{-1}$, respectively[23]. Compared with other studies with modified MO husks, the BET specific surface area of H-MOH300 substantially increased (Table 3). This can be associated with the method of preparation of the adsorbent. Quesada et al.[25] prepared an adsorbent from MO seed husk modified with phosphoric acid at 300°C. However, the precursor was washed before the heating process, unlike the H-MO used in this study, which was washed only after thermal activation. The presence of phosphoric acid during thermal activation may explain the larger surface area of H-MOH300. In their research, chemical activation was performed with a ratio of 30 g to 1 L of 0.1 mol L^{-1} phosphoric acid for 3 h, whereas H-MOH300 was activated with a 1:5 (m/v) ratio for 1 h. Another difference to be considered is the separation by particle size; they used particles between 500 and 600 µm[25], and the particle size distribution of H-MOH300 is from 0.04 µm to 600 µm, with an 88.8 µm D50 and 294.2 µm D90 (Figure 3). These differences could explain the difference in the BET specific surface area between the two adsorbents, especially the particle size, since a study with BPA adsorption showed that as the particle size increased, the sorption capacity decreased[47].

3.2.2. Surface morphology and crystallinity

The SEM image (Figure 4) shows heterogeneous morphological characteristics, and the porous and fibrous structures presented agree with previous observations[24,25,46]. The surface presents some pores that are 4.06 ± 1.62 µm in size connected to the inside of the fibres, which explains the isotherm type and lack of overlap of N_2 desorption (Figure 2).

The X-ray diffractogram presented in Figure 5 shows a defined peak at 2θ = 25°, indicating the presence of an alignment of the material layers[46]. The calculated crystallinity index (CI) is 78.0%, suggesting a predominantly crystalline nature of the material. An elevation is also observed at 2θ = 45°. It cannot be considered a peak, but its presence can be explained by the heterogeneity and complexity of the adsorbent [46]. This elevation could be associated with disordered layers of graphite formed during the activation process[48].

3.2.3. FTIR spectroscopy

The Fourier transform infrared spectra are shown in Figure 6, in which the functional groups present in H-MOH300 were determined before and after BPA adsorption. The broad peak at 3342 cm^{-1} indicates the presence of O–H hydroxyl bonds [25,49,50]. The band at 1589 cm^{-1} indicates the presence of aromatic rings[25]. Furthermore, the peak at 1232 cm^{-1} is associated with C–O groups[25], which, along with the O–H band, may indicate the presence of carboxylic functional

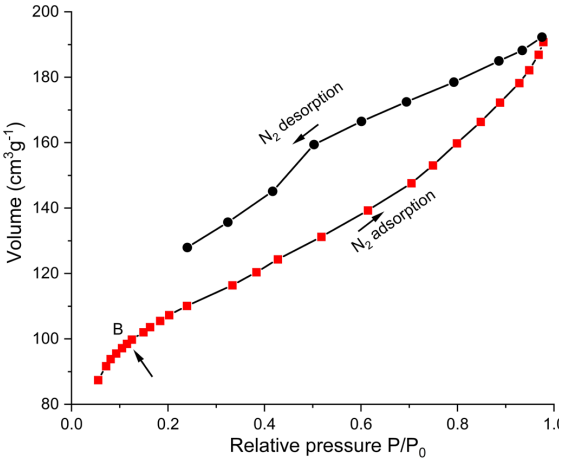

Figure 2. N_2 physisorption isotherm for H-MOH300.

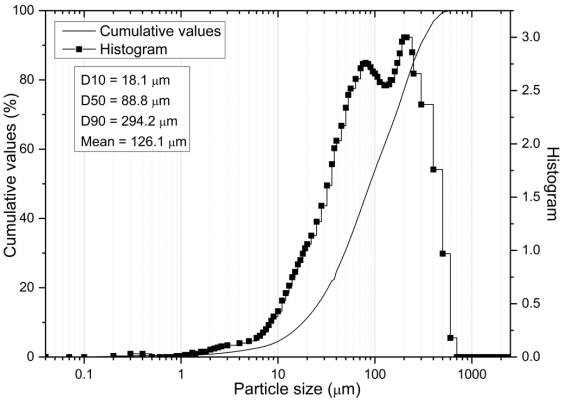

Figure 3. Particle size distribution of H-MOH300 (cumulative curve and histogram).

Table 3. BET specific surface areas of different modified *Moringa oleifera* seed husk adsorbents.

Modification Method	BET specific surface area ($m^2\ g^{-1}$)	Reference
Without modification	3.24	23
H_3PO_4 at 300°C	4.6	25
Methanol, HNO_3 at 300°C	5.77	46
Methanol, HNO_3 at 300°C	10.32	24
H_3PO_4 at 300°C	380	This study

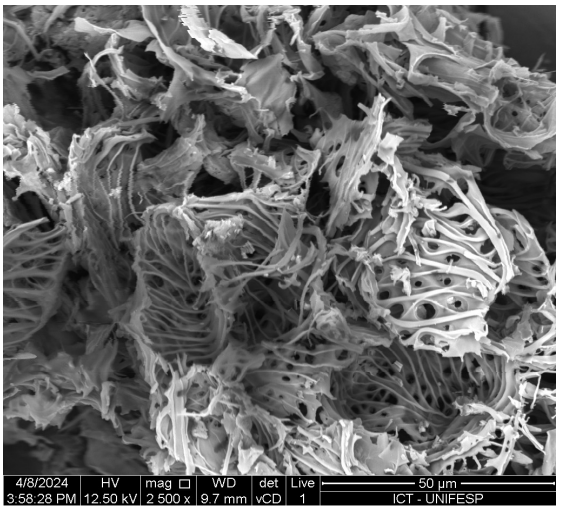

Figure 4. Scanning electron microscopy image of H-MOH300.

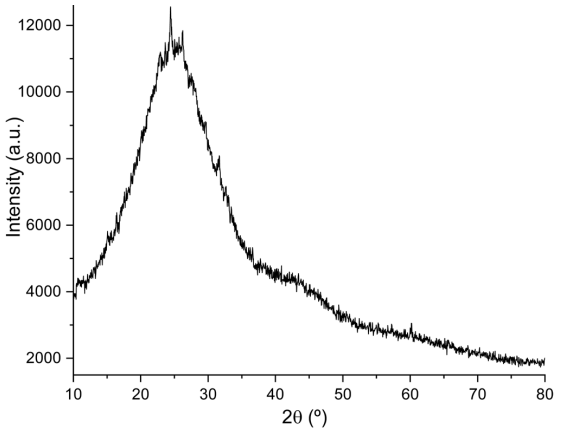

Figure 5. X-ray diffractogram of H-MOH300.

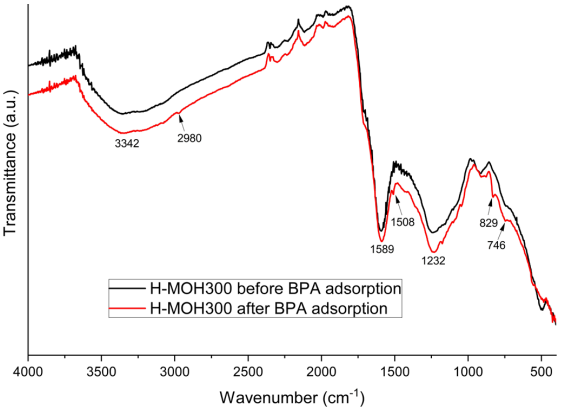

Figure 6. FITR spectra of H-MO300 before and after BPA adsorption.

groups. After BPA adsorption, additional peaks related to BPA molecules can be observed. The peak at 2980 cm^{-1} is possibly associated with C–H bonds. The peak at 1508 cm^{-1} is related to H–C–H interactions outside the aromatic rings; the peak at 829 cm^{-1} could be related to C–O stretching and C–C stretching in both the rings and from C–H out-of-plane bending movements. In addition, the peak at 746 cm^{-1} could be caused by C–C stretching in BPA molecules[51].

3.2.4. Point of zero charge (pH_{PZC}) and the effect of the pH on the adsorption process

The pH_{PCZ} analysis of H-MOH300 is shown in Figure 7. The pH_{PZC} of approximately 4.5 is the neutral loading point of H-MOH300. The pH_{PZC} value is important to consider when studying the adsorption process. If the solution pH exceeds the pH_{PZC} value, the functional groups of the adsorbent become deprotonated, leading to a negatively charged surface, which enhances the adsorption of cationic adsorbates[23]. For H-MOH300, deprotonation is favoured due to the low pH_{PZC} value, indicating that the protons are weakly bonded to the functional groups. This is because the driving force in the solution, which is composed of anionic groups such as OH^- and NO_3^-, is strong enough to eliminate them. At pH values below the pH_{PZC}, the positive charge developed on the adsorbent surface is smaller than that at pH values above the pH_{PZC}. This suggests that the functional groups responsible for increasing the pH are more strongly bonded to the adsorbent surface and that the driving force of the solution (e.g., H^+ and Na^+) cannot displace them. This observation is consistent with the FTIR results (Figure 6), which indicate the presence of carboxylic groups and explain the pH_{PZC} profile.

The *pKa* values of BPA range from 9.6–10.2[52,53]. This means that when the pH is higher than the pKa, the BPA molecule can undergo ionization to form a bisphenol anion. This leads to electrostatic repulsion between the negatively charged carbon surface and the bisphenol anion, which reduces the adsorption of BPA onto the adsorbent. However, when the pH is lower than the pKa, BPA adsorption remains at its highest level and nearly constant because BPA is undissociated. At this pH, the adsorptive interaction between the undissociated BPA molecules and the adsorbent is the main factor[53]. Figure 8 shows the results for the pH effect. The significant reduction in adsorption capacity at pH values exceeding 8.2 can be attributed to electrostatic repulsion. This repulsion arises from the negative charges on the surface of the adsorbent, which has a pH_{PZC} of 4.5, and BPA, which has a *pKa* ranging between 9.6 and 10.2. At higher pH values, the adsorbent and BPA molecules become negatively charged, resulting in repulsive interactions that hinder effective adsorption. Considering that tests with pH values between 5.9 and 6.6 presented approximately the same q_e, a pH of 6.0 was chosen for the subsequent experiments since there was no need for pH correction.

3.3. Adsorption studies

3.3.1. Adsorbent dosage effect on the adsorption capacity

The effect of the H-MOH300 concentration on the capacity for BPA adsorption is shown in Figure 9. At initial concentrations, the percentage of BPA removal increases sharply as the adsorbent dosage increases. This increase could be linked to the greater quantity of active adsorption sites available on the adsorbent[18]. The adsorption capacity

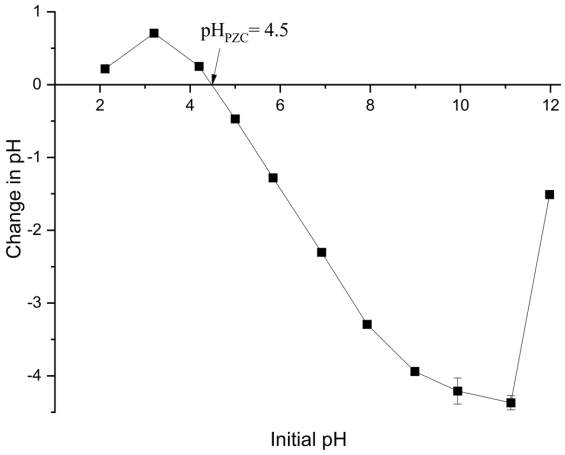

Figure 7. Point of zero charge (pH$_{PZC}$) of H-MOH300.

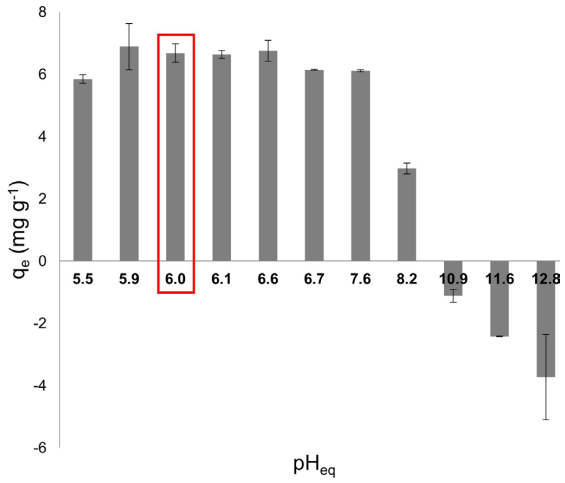

Figure 8. Effect of the pH on the BPA adsorption of H-MOH300 (C$_0$ = 20 mg L^{-1}, 22°C, V = 50 mL, H-MOH300 dosage = 2.0 g L^{-1}, 1440 min, 100 rpm).

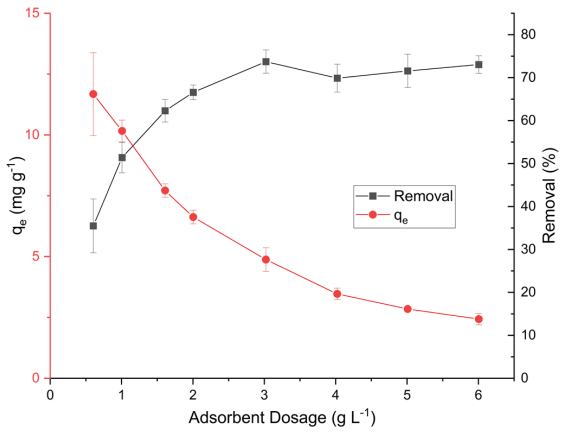

Figure 9. H-MOH300 dosage effect on BPA adsorption (C$_0$ = 20 mg L^{-1}, 22°C, V = 50 mL, pH = 6.0, 1440 min, 100 rpm).

values (q$_e$) decreased as the H-MOH300 concentration increased. This can be attributed to the larger quantity and greater availability of binding sites as the adsorbent mass increases. As a result, determining the maximum adsorption capacity is not possible because the remaining sites are not saturated[25]. The maximum removal of 74 ± 2% was achieved at a dosage of 3 g L^{-1}. At a dosage of 2 g L^{-1}, a BPA removal efficiency of 69 ± 3% was attained, and further increasing the dosage did not significantly improve the removal efficiency. Therefore, using 2 g L^{-1} adsorbent is economically justified and was selected for this study.

3.3.2. Adsorption isotherms

Figure 10 shows the experimental data obtained at 22°C, 32°C, and 42°C by plotting the BPA adsorbed on H-MOH300 at equilibrium (q$_e$) versus the equilibrium BPA concentration in solution (C$_e$). The maximum adsorption capacity improved with increasing temperature. The isotherm equations provide the parameters outlined in Table 4. Furthermore, the suitability of these equations was assessed via the most suitable statistical parameters (R^2 and χ^2) for equilibrium curves.

Based on the information in Table 4, the Langmuir model provided the best fit for the three temperatures tested (higher R^2 and lower χ^2), achieving maximum capacity (q$_{max}$) of 27.5 ± 1.3 mg g^{-1} at 22°C. This suggests that the adsorption surface is uniform, that the adsorption takes place at specific locations, and that the maximum adsorption indicates saturation of the monolayer[47].

3.3.3. Comparison of H-MOH300 with other adsorbents

The adsorption performance of H-MOH300 was evaluated against various natural agricultural waste-derived adsorbents used for BPA removal from water. Table 5 provides a comparative analysis, considering key parameters such as maximum adsorption capacity (q$_{max}$), optimal pH, and equilibrium time.

H-MOH300 demonstrated a superior adsorption capacity (27.5 mg g^{-1}) compared to most natural adsorbents, outperforming materials such as barley husk (15.51 mg g^{-1})[54], rice husk ash (2.65 mg g^{-1})[55], and reed straws (1.72 mg g^{-1})[49]. Additionally, unlike several adsorbents that require pH adjustments to acidic conditions, H-MOH300 operated efficiently at near-neutral pH (pH 6.0), enhancing its practical applicability.

However, the adsorption equilibrium time for H-MOH300 (960 min) was longer than that of many other adsorbents, such as $ZnCl_2$ activated *Moringa oleifera* pods (60 min)[50], Cellulose fibres-Spanishbroom plant (60 min)[13] and HCl-treated barley husk (90 min)[54]. This extended equilibrium time may influence its large-scale application, where rapid adsorption kinetics are desirable. Despite this limitation, the high adsorption capacity and mild pH requirement highlight H-MOH300's potential as an effective and sustainable solution for BPA removal from contaminated water sources.

3.3.4. Thermodynamic study

Studying the thermodynamic process of adsorption is important for understanding how adsorption works and whether

adsorption is through physical or chemical mechanisms. Specific thermodynamic parameters, such as the change in Gibbs energy (ΔG°), enthalpy (ΔH°), and entropy (ΔS°), can distinguish physical from chemical adsorption[56]. As the experimental equilibrium data (Figure 10) indicated a dependence on temperature, the thermodynamic parameters of the BPA adsorption process onto H-MOH300 were investigated via the Langmuir model, which best fitted the experimental data. Table 6 lists the calculated values of ΔG°, ΔH°, and ΔS°. The parameter K_C was calculated using the K_L constant from the Langmuir model via Equation 13.

The change in Gibbs energy is crucial in deciding how spontaneous the adsorption process is. If the Gibbs energy is negative, the adsorption process will occur favourably and spontaneously at a given temperature[55], as presented for H-MOH300. The Gibbs energy also decreases with increasing temperature, which implies that BPA removal is favoured with increasing heat. The positive enthalpy shows that the BPA adsorption process with H-MOH300 absorbs heat, making it an endothermic process. An enthalpy of less than 20 kJ mol^{-1} indicates physisorption[57]. The positive entropy value suggests that the organization of the adsorbate at the solid/solution interface becomes more random, indicating a dissociative mechanism. Other authors have also reported that the adsorption of BPA is endothermic, with an enthalpy value indicating physisorption and positive values for the change in entropy (ΔS°)[15,18].

3.3.5. Adsorption kinetics

The kinetics of the adsorption data were analysed via the pseudo-first-order, pseudo-second-order, intraparticle diffusion, and Elovich kinetic models. The results are illustrated in Figure 11, and the corresponding parameters are provided in Table 7. The adsorption capacity of H-MOH300 for BPA increases and becomes stable with a contact time of 960 min (q_e = 8.20 mg g^{-1}). On the basis of

Table 4. Isotherm model parameters of equilibrium adsorption data for BPA onto H-MOH300.

Isotherm Model	Parameters	22°C	32°C	42°C
Langmuir	q_{max} (mg g^{-1})	27.5 ± 1.3	27.9 ± 1.6	32.7 ± 1.8
	K_L (L mg^{-1})	0.048 ± 0.006	0.049 ± 0.008	0.052 ± 0.007
	R^2	0.9815	0.9690	0.9727
	χ^2	0.7359	1.2245	1.3185
Freundlich	K_F (mg g^{-1})	3.1 ± 0.5	3.2 ± 0.6	3.8 ± 0.5
	n	2.1 ± 0.2	2.2 ± 0.2	2.1 ± 0.2
	R^2	0.9509	0.9339	0.9660
	χ^2	1.9494	2.6133	1.6395
Temkin	K_T (L mg^{-1})	0.53 ± 0.07	0.50 ± 0.07	0.57 ± 0.08
	b_T (J mol^{-1})	419 ± 22	416 ± 22	376 ± 22
	R^2	0.9709	0.9691	0.9639
	χ^2	1.1567	1.2220	1.7411

Table 5. Comparison of the maximum adsorption capacity of adsorbents from different sources for BPA.

Absorbents	Modification Method	Equilibrium time (min)	pH	q_{max} (mg g^{-1})	Reference
MO pods	$ZnCl_2$ at 500°C	60	7	20.14	[50]
Barley husk	HCl, dried at 105°C	90	3	15.51	[54]
Cellulose fibres-Spanishbroom plant (FF)	Hydrophobization with MDI	60	5	4.86	[13]
Rice husk ash	-	180	6	2.65	[55]
Reed straws	K_3PO_4 at 500°C	1440	Not informed	1.72	[49]
MO husk seed	H_3PO_4 at 300°C	960	6	27.5	This study

Table 6. Thermodynamic parameters of BPA adsorption using H-MOH300 as the adsorbent.

Temperature (°C)	K_C	ΔG° (kJ mol^{-1})	ΔH° (kJ mol^{-1})	ΔS° (J $mol^{-1}K^{-1}$)	Van't Hoff equation
22	611,965	-32.7	2.9	120.6	Y=-350.3x+14.5 R^2 = 0.93
32	624,635	-33.9			
42	660,111	-35.1			

the regression coefficients R^2, error function analyses (χ^2), and proximity of the experimentally determined q_t values to the theoretical values, the pseudo-second-order kinetic model was clearly preferable, indicating that physical interactions occurred between the adsorbent and adsorbate[58]. This model also accurately represents the kinetics data for other BPA adsorption processes[15,49,50].

3.4. Mechanisms of adsorption

Based on the dataset discussed, BPA removal by H-MOH300 primarily occurs through electrostatic interactions. This is supported by the increased adsorption capacity at pH values above the pH_{PZC} and below the BPA pKa. At a pH of 6.0, the adsorbent surface is partially negative, as indicated by the pH_{PZC} profile (Figure 7), suggesting the presence of both protonated and nonprotonated functional groups. According to the FTIR analysis after adsorption (Figure 6), the O–H functional groups were not suppressed, and C–O and H–C–H functional groups were observed. The electrostatic potential map of BPA[59] indicates that the carbons in the ring are likely bonded to both nonprotonated and protonated adsorbent surface groups, whereas the oxygen atoms are bound to protonated groups and to the hydrogen of the OH functional group of BPA. The proposed adsorption mechanism between BPA and H-MOH300 is illustrated in Figure 12. Other authors have reported similar conclusions regarding the adsorption of BPA by agricultural waste adsorbents[31,49,60]. The calculated $\Delta H°$ (2.9 kJ mol^{-1}) also supports the hypothesis that these interactions are primarily electrostatic, indicative of physisorption with no electron sharing or exchange. On the basis of the FTIR spectra (Figure 6), the O–H groups of H-MOH300 could interact with BPA molecules through dipole–dipole hydrogen bonds, and the aromatic rings in both H-MOH300 and BPA structures can also favour π–π interactions[45].

3.5. Regeneration study

The regeneration capacity of an adsorbent corroborates its effectiveness, stability, and reusability for adsorption, as well as its economic feasibility[19]. Figure 13 shows the H-MOH300 regeneration capacity for BPA adsorption after five cycles. The adsorption capacity of H-MOH300 decreases by approximately 11 % after the fifth cycle of reuse, ranging from 22.5 ± 3.7 to 20.1 ± 2.6 mg g^{-1}. These results demonstrated the capacity of H-MOH300 to be restored and utilized multiple times in water treatment processes, similar to other adsorbents investigated for BPA removal in the recent literature[15,18,19].

Table 7. Kinetic model parameters for BPA adsorption when H-MOH300 was used as the adsorbent.

Kinetic Models	Estimated parameters	Experimental data H-MOH300
Pseudo-first-order	q_{eq} (mg g^{-1})	7.8 ± 0.3
	k_1 (min^{-1})	0.031 ± 0.005
	R^2	0.9909
	χ^2	61.463
Pseudo-second-order	q_{eq} (mg g^{-1})	8.6 ± 0.3
	k_2 (g mg^{-1} min^{-1})	0.005 ± 0.001
	R^2	0.9924
	χ^2	51.218
Intraparticle diffusion model	K_{dif} (mg g^{-1} $min^{-0.5}$)	0.11 ± 0.04
	C (mg g^{-1})	4.5 ± 0.9
	R^2	0.4623
	χ^2	2.939
Elovich model	α (mg g^{-1} min^{-1})	207 ± 232
	β (mg g^{-1})	1.5 ± 0.2
	R^2	0.9816
	χ^2	0.101

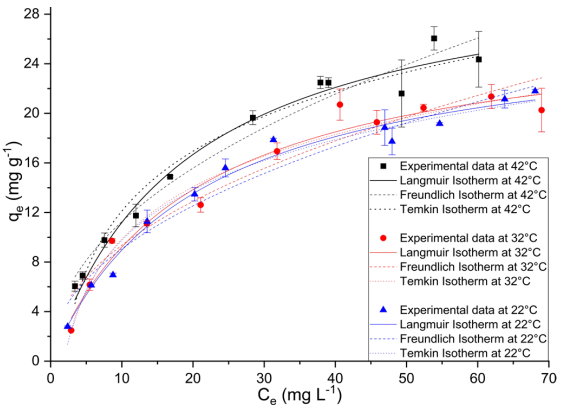

Figure 10. Adsorption isotherms for BPA adsorption using H-MOH300 as an adsorbent at different temperatures (V = 50 mL, H-MOH300 dosage = 2.0 g L^{-1}, pH = 6.0, 960 min, 100 rpm).

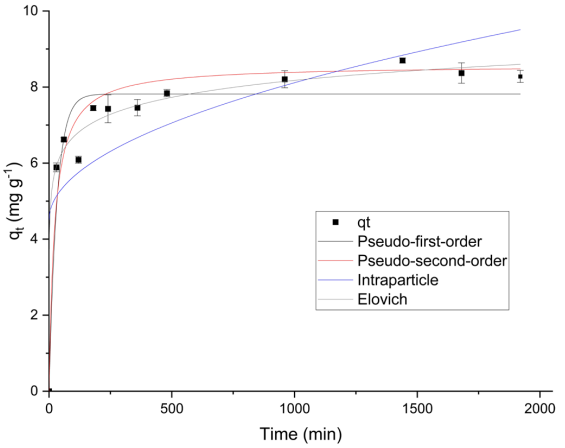

Figure 11. Kinetics of BPA adsorption using H-MOH300 as an adsorbent (C_0 = 20 mg L^{-1}, 22°C, V = 50 mL, H-MOH300 dosage = 2.0 g L^{-1}, pH = 6.0, 100 rpm).

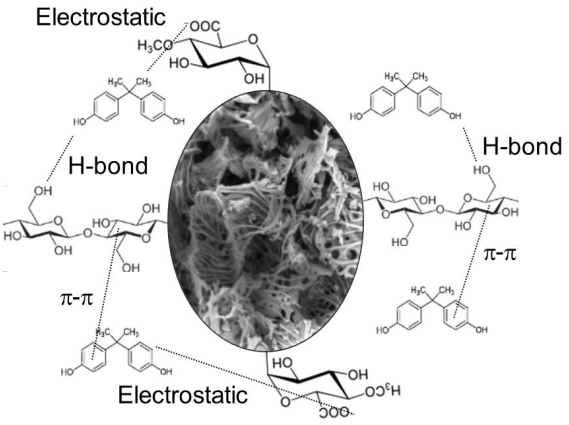

Figure 12. Proposed mechanism of BPA adsorption onto H-MOH300.

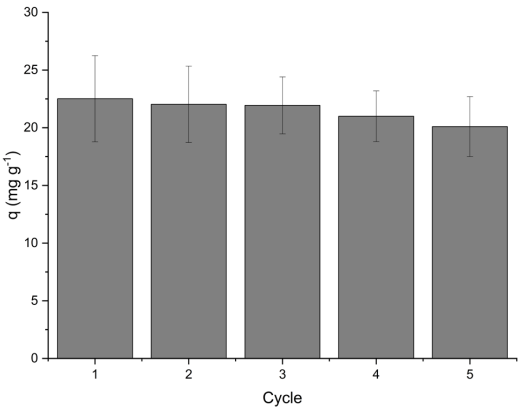

Figure 13. Regeneration of H-MOH300 for BPA adsorption from water during five cycles of adsorption–desorption (C_0 = 120 mg L^{-1}, 22°C, V = 250 mL, H-MOH300 dosage = 2.0 g L^{-1}, pH = 6.0, 960 min, 100 rpm).

4. Conclusion

This research assessed the bisphenol A (BPA) adsorption capacity of an adsorbent prepared with *Moringa oleifera* seed husks chemically activated with phosphoric acid and thermally activated at 300°C. The BET-specific surface area and total pore volume of 380 m^2 g^{-1} and 0.282 cm^3 g^{-1}, respectively, indicate successful activation compared with the *M. oleifera* seed husk activation reported in the literature. Scanning electron microscopy (SEM) revealed a porous and fibrous structure, while XRD indicated a crystalline nature. Fourier transform infrared spectroscopy (FTIR) identified key functional groups, including hydroxyl, aromatic, and carboxylic groups, that play a role in BPA binding. The Langmuir model isotherm provided the best fit for the three temperatures tested, indicating a favourable adsorption process with a maximum adsorption capacity of 27.5 ± 1.3 mg g^{-1} at 22°C, which is higher than that reported in some agricultural waste adsorbent studies on the removal of BPA recently published in the literature. The adsorption kinetics were best described by the pseudo-second-order model, indicating that the process is endothermic, with a $\Delta H°$ of 2.9 kJ mol^{-1}, indicating physisorption. The adsorption process is also spontaneous, with a $\Delta G°$ ranging from -35.1 to -32.7 kJ mol^{-1}. The results also suggest that the adsorption mechanisms are mainly electrostatic, with some hydrogen bonds and π–π interactions.

The regeneration study demonstrated that H-MOH300 retained 89% of its adsorption capacity up to 5 adsorption-desorption cycles, reinforcing its potential for reuse in water treatment applications. The ability to regenerate the material without a significant loss in performance enhances its economic viability and sustainability as a low-cost alternative to conventional adsorbents. Additionally, compared to other agricultural waste-derived adsorbents, H-MOH300 exhibited a higher adsorption capacity while operating effectively at near-neutral pH, eliminating the need for pH adjustments that could complicate large-scale applications.

However, some limitations must be considered. The adsorption equilibrium time for H-MOH300 (960 min) was longer than that of other adsorbents, which could be a disadvantage in practical applications requiring rapid treatment. Further research should focus on optimizing the adsorption kinetics to enhance process efficiency. Moreover, while the study was conducted under controlled laboratory conditions, real water matrices often contain a complex mixture of contaminants, natural organic matter, and competing ions that may influence adsorption performance. Future studies should evaluate the adsorbent's efficiency in real-world scenarios, such as wastewater treatment plants or industrial effluents, to better understand its applicability under variable environmental conditions.

Despite these challenges, this study highlights the potential of H-MOH300 as a promising eco-friendly and cost-effective material for removing BPA from contaminated water sources. The valorization of agricultural residues as functional adsorbents not only contributes to the development of sustainable water treatment technologies but also provides an environmentally responsible solution for repurposing agro-industrial waste.

5. Acknowledgments

This study was financed, in part, by the São Paulo Research Foundation (FAPESP), Brasil. Process Number 2024/06591-5 and by The National Council for Scientific and Technological Development (CNPq) (PIBIC number 120902/2023-0).

6. References

1. Zhou Y, Wang Z, Xia M, Zhuang S, Gong X, Pan J, et al. Neurotoxicity of low bisphenol A (BPA) exposure for young male mice: implications for children exposed to environmental levels of BPA. Environ Pollut. 2017;229:40-8. http://doi.org/10.1016/j.envpol.2017.05.043. PMid:28577381.
2. Ohore OE, Zhang S. Endocrine disrupting effects of bisphenol A exposure and recent advances on its removal by water treatment systems. A review. Sci African. 2019;e00135. https://doi.org/10.1016/j.sciaf.2019.e00135.
3. Alonso-Magdalena P, Ropero AB, Soriano S, García-Arévalo M, Ripoll C, Fuentes E, et al. Bisphenol-A acts as a potent estrogen via non-classical estrogen triggered pathways. Mol Cell Endocrinol. 2012;355(2):201-7. http://doi.org/10.1016/j.mce.2011.12.012. PMid:22227557.

4. Abu Hasan H, Muhamad MH, Budi Kurniawan S, Buhari J, Husain Abuzeyad O. Managing Bisphenol A Contamination: Advances in Removal Technologies and Future Prospects. Water. 2023;15(20):1-34. http://doi.org/10.3390/w15203573.
5. Martini GA, Montagner CC, Viveiros W, Quinaglia GA, França DD, Munin NCG, et al. Emerging contaminant occurrence and toxic effects on zebrafish embryos to assess the adverse effects caused by mixtures of substances in the environment. Environ Sci Pollut Res Int. 2021;28(16):20313-29. http://doi.org/10.1007/s11356-020-11963-x. PMid:33405144.
6. Madeira CL, Acayaba RDA, Santos VS, Villa JEL, Jacinto-Hernández C, Azevedo JAT, et al. Uncovering the impact of agricultural activities and urbanization on rivers from the Piracicaba, Capivari, and Jundiaí basin in São Paulo, Brazil: A survey of pesticides, hormones, pharmaceuticals, industrial chemicals, and PFAS. Chemosphere. 2023;341:341. http://doi.org/10.1016/j.chemosphere.2023.139954. PMid:37660794.
7. Sabino JA, de Sá Salomão AL, de Oliveira Muniz Cunha PM, Coutinho R, Marques M. Occurrence of organic micropollutants in an urbanized sub-basin and ecological risk assessment. Ecotoxicology. 2021;30(1):130-41. http://doi.org/10.1007/s10646-020-02304-2. PMid:33175334.
8. Corrêa JMM, Sanson AL, Machado CF, Aquino SF, Afonso RJCF. Occurrence of contaminants of emerging concern in surface waters from Paraopeba River Basin in Brazil: seasonal changes and risk assessment. Environ Sci Pollut Res Int. 2021;28(23):30242-54. http://doi.org/10.1007/s11356-021-12787-z. PMid:33586100.
9. Roledo C, França DD, dos Santos Feitosa IR, Quinaglia GA, Montagner CC, Roubicek DA, et al. A comprehensive study on bisphenol A and estrogenic activity in the Paraíba do Sul River, São Paulo, Brazil. J Water Health. 2024;22(11):2060-75. http://doi.org/10.2166/wh.2024.205. PMid:39611669.
10. Lima DRS, Tonucci MC, Libânio M, de Aquino SF. Fármacos e desreguladores endócrinos em águas Brasileiras: ocorrência e técnicas de remoção. Eng Sanit Ambient. 2017;22(6):1043-54. http://doi.org/10.1590/s1413-41522017165207.
11. Padhye LP, Yao H, Kung'u FT, Huang CH. Year-long evaluation on the occurrence and fate ofpharmaceuticals, personal care products, andendocrine disrupting chemicals in an urban drinking water treatment plant. Water Res. 2014;51:266-76. http://doi.org/10.1016/j.watres.2013.10.070. PMid:24262763.
12. IBGE: Instituto Brasileiro de Geografia e Estatística. Pesquisa Nacional de Saneamento Básico 2017 [Internet]. Rio de Janeiro: IBGE; 2017 [cited 2023 May 25]. Available from: https://cidades.ibge.gov.br/brasil/pesquisa/30/84366
13. Tursi A, Chatzisymeon E, Chidichimo F, Beneduci A, Chidichimo G. Removal of endocrine disrupting chemicals from water: adsorption of bisphenol-a by biobased hydrophobic functionalized cellulose. Int J Environ Res Public Health. 2018;15(11):2419. http://doi.org/10.3390/ijerph15112419. PMid:30384467.
14. Mpatani FM, Han R, Aryee AA, Kani AN, Li Z, Qu L. Adsorption performance of modified agricultural waste materials for removal of emerging micro-contaminant bisphenol A: a comprehensive review. Sci Total Environ. 2021;780:146629. http://doi.org/10.1016/j.scitotenv.2021.146629. PMid:34030339.
15. Chen A, Xie Y, Wei X, Chen B, Pang J. One-step preparation of sodium alginate-based porous carbon for the adsorption of bisphenol a in water. J Chem Eng Data. 2021;66(2):1101-9. http://doi.org/10.1021/acs.jced.0c00894.
16. Naganathan KK, Faizal ANM, Zaini MAA, Ali A. Adsorptive removal of Bisphenol a from aqueous solution using activated carbon from coffee residue. Mater Today Proc. 2020;47:1307-12. http://doi.org/10.1016/j.matpr.2021.02.802.
17. Saha B, Gayen S, Debnath A. Sequestration of Paracetamol from Aqueous Solution Using Zinc Oxide/Polypyrrole Nanocomposite: Cost Analysis, Scale-Up Design, and Optimization of Process Parameters. J Hazard Toxic Radioact Waste. 2023;27(4):1-16. http://doi.org/10.1061/JHTRBP.HZENG-1213.
18. Vidovix TB, Januário EFD, Bergamasco R, Vieira AMS. Bisfenol A adsorption using a low-cost adsorbent prepared from residues of babassu coconut peels. Environ Technol. 2021;42(15):2372-84. http://doi.org/10.1080/09593330.2019.1701568. PMid:31801431.
19. Mpatani FM, Aryee AA, Kani AN, Guo Q, Dovi E, Qu L, et al. Uptake of micropollutant-bisphenol A, methylene blue and neutral red onto a novel bagasse-β-cyclodextrin polymer by adsorption process. Chemosphere. 2020;259:127439. http://doi.org/10.1016/j.chemosphere.2020.127439. PMid:32593825.
20. Ribeiro JVM, Andrade PV, dos Reis AG. *Moringa oleifera* seed as a natural coagulant to treat low-turbidity water by in-line filtration. Rev Ambient Água. 2019;14(6):e2442. https://doi.org/10.4136/ambi-agua.2442.
21. Batista GS, Roledo C, Odjegba EE, Fiore FA, Moruzzi RB, Reis AG. *Moringa oleifera* seed addition prior to sludge thickening for supernatant quality improvement: analyses of clarification performance and toxicity. Sustain. 2023;15(9):7288. https://doi.org/10.3390/su15097288.
22. Chales GG, Tihameri BS, Milhan NVM, Koga-Ito CY, Antunes MLP, dos Reis AG. Impact of *Moringa oleifera* seed-derived coagulants processing steps on physicochemical, residual organic, and cytotoxicity properties of treated water. Water. 2022;14(13):2058. http://doi.org/10.3390/w14132058.
23. Lopes CA, Roledo C, dos Reis AG. *Moringa oleifera* seed husks for methylene blue dye adsorption: kinetic, equilibrium, and thermodynamic analyses. Rev Ambient Água. 2022;17(1):e2812. https://doi.org/10.4136/ambi-agua.2812.
24. Cusioli LF, Bezerra CO, Quesada HB, Alves Baptista AT, Nishi L, Vieira MF, et al. Modified *Moringa oleifera* Lam. Seed husks as low-cost biosorbent for atrazine removal. Environ Technol. 2021;42(7):1092-103. http://doi.org/10.1080/09593330.2019.1653381. PMid:31412750.
25. Quesada HB, Cusioli LF, de O Bezerra C, Baptista ATA, Nishi L, Gomes RG, et al. Acetaminophen adsorption using a low-cost adsorbent prepared from modified residues of *Moringa oleifera* Lam. seed husks. J Chem Technol Biotechnol. 2019;94(10):3147-57. http://doi.org/10.1002/jctb.6121.
26. Yamaguchi NU, Cusioli LF, Quesada HB, Ferreira MEC, Fagundes-Klen MR, Vieira AMS, et al. A review of *Moringa oleifera* seeds in water treatment: trends and future challenges. Process Saf Environ Prot. 2021;147:405-20. http://doi.org/10.1016/j.psep.2020.09.044.
27. Zbair M, Ainassaari K, Drif A, Ojala S, Bottlinger M, Pirilä M, et al. Toward new benchmark adsorbents: preparation and characterization of activated carbon from argan nut shell for bisphenol A removal. Environ Sci Pollut Res Int. 2018;25(2):1869-82. http://doi.org/10.1007/s11356-017-0634-6. PMid:29103116.
28. Acosta R, Nabarlatz D, Sánchez-Sánchez A, Jagiello J, Gadonneix P, Celzard A, et al. Adsorption of Bisphenol A on KOH-activated tyre pyrolysis char. J Environ Chem Eng. 2018;6(1):823-33. http://doi.org/10.1016/j.jece.2018.01.002.
29. Das J, Mondal A, Biswas S, Nag S. The eco-friendly treatment of rubber industry effluent by using adsorbent derived from *Moringa oleifera* bark and Pseudomonas sp, cultured from effluent. Water Sci Technol. 2022;86(11):2808-19. http://doi.org/10.2166/wst.2022.387. PMid:36515190.
30. Bakatula EN, Richard D, Neculita CM, Zagury GJ. Determination of point of zero charge of natural organic materials. Environ Sci Pollut Res Int. 2018;25(8):7823-33. http://doi.org/10.1007/s11356-017-1115-7. PMid:29294236.
31. Rovani S, Santos JJ, Guilhen SN, Corio P, Fungaro DA. Fast, efficient and clean adsorption of bisphenol-A using renewable mesoporous silica nanoparticles from sugarcane waste ash. RSC Advances. 2020;10(46):27706-12. http://doi.org/10.1039/D0RA05198E. PMid:35516950.

32. Zbair M, Bottlinger M, Ainassaari K, Ojala S, Stein O, Keiski RL, et al. Hydrothermal Carbonization of Argan Nut Shell: Functional Mesoporous Carbon with Excellent Performance in the Adsorption of Bisphenol A and Diuron. Waste Biomass Valoriz. 2020;11(4):1565-84. http://doi.org/10.1007/s12649-018-00554-0.
33. Zhong P, Qiu X, Chen J. Removal of bisphenol A using Mg-Al-layer double hydroxide and Mg-Al calined layer double hydroxide. Sep Sci Technol. 2020;55(3):501-12. http://doi.org/10.1080/01496395.2019.1577265.
34. Deb A, Debnath A, Saha B. Sono-assisted enhanced adsorption of eriochrome Black-T dye onto a novel polymeric nanocomposite : kinetic, isotherm, and response surface methodology optimization. J Dispers Sci Technol. 2021;0(0):1-14. http://doi.org/10.1080/01932691.2020.1775093.
35. Lagergren SY. About the theory of so-called adsorption of solid substance. Handlingar. 1898;4:1-39.
36. Ho YS, McKay G. Pseudo-second order model for sorption processes. Process Biochem. 1999;34(5):451-65. http://doi.org/10.1016/S0032-9592(98)00112-5.
37. Weber WJ Jr, Morris JC. Kinetics of adsorption on carbon from solution. J Sanit Engrg Div. 1963;89(2):31-60. http://doi.org/10.1061/JSEDAI.0000430.
38. McLintock IS. The elovich equation in chemisorption kinetics. Nature. 1967;216(5121):1204-5. http://doi.org/10.1038/2161204a0.
39. Langmuir I. The constitution and fundamental properties of solids and liquids. J Am Chem Soc. 1916;38(11):2221-95. http://doi.org/10.1021/ja02268a002.
40. Freundlich H. Over the adsorption in solution. J Phys Chem. 1906;57:385-470.
41. Temikn M, Pyzhev V. Recent modifications to Langmuir isotherms. Acta Physiochim URSS. 1940;12:217-22.
42. Tran HN, You SJ, Hosseini-Bandegharaei A, Chao HP. Mistakes and inconsistencies regarding adsorption of contaminants from aqueous solutions: A critical review. Water Res. 2017;120:88-116. http://doi.org/10.1016/j.watres.2017.04.014. PMid:28478298.
43. Mustapha S, Shuaib DT, Ndamitso MM, Etsuyankpa MB, Sumaila A, Mohammed UM, et al. Adsorption isotherm, kinetic and thermodynamic studies for the removal of Pb (II), Cd (II), Zn (II) and Cu (II) ions from aqueous solutions using Albizia lebbeck pods. Appl Water Sci. 2019;9(6):1-11. http://doi.org/10.1007/s13201-019-1021-x.
44. Zhou X, Zhou X. The Unit problem in the thermodynamic calculation of adsorption using the Langmuir Equation. Chem Eng Commun. 2014;201(11):1459-67. http://doi.org/10.1080/00986445.2013.818541.
45. Zbair M, Ainassaari K, El Assal Z, Ojala S, El Ouahedy N, Keiski RL, et al. Steam activation of waste biomass: highly microporous carbon, optimization of bisphenol A, and diuron adsorption by response surface methodology. Environ Sci Pollut Res Int. 2018;25(35):35657-71. http://doi.org/10.1007/s11356-018-3455-3. PMid:30353441.
46. Bezerra CO, Cusioli LF, Quesada HB, Nishi L, Mantovani D, Vieira MF, et al. Assessment of the use of *Moringa oleifera* seed husks for removal of pesticide diuron from contaminated water. Environ Technol. 2020;41(2):191-201. http://doi.org/10.1080/09593330.2018.1493148. PMid:29932815.
47. Jiang Y, Yuan L, Liu L, Shi L, Guang A, Mu Z. Bisphenol A in the Yellow River: sorption characteristics and influential factors. J Hydrol (Amst). 2018;564:307-13. http://doi.org/10.1016/j.jhydrol.2018.06.079.
48. Duan X, Srinivasakannan C, Wang X, Wang F, Liu X. Synthesis of activated carbon fibers from cotton by microwave induced H3PO4 activation. J Taiwan Inst Chem Eng. 2017;70:374-81. http://doi.org/10.1016/j.jtice.2016.10.036.
49. Zhao Y, Yang M, Qi K, Pan J. The adsorption of bisphenol A by biochars modified with potassium phosphate. Desalination Water Treat. 2024;319:100444. http://doi.org/10.1016/j.dwt.2024.100444.
50. Hussain NB, Akgül ET, Yılmaz M, Parlayıcı Ş, Hadibarata T. Preparation and characterization of low-cost activated carbon from *Moringa oleifera* chemically activated using ZnCl2 for the adsorption of bisphenol A. Int J Phytoremediation. 2023;25(9):1199-214. http://doi.org/10.1080/15226514.2022.2144796. PMid:36437736.
51. Ullah R, Ahmad I, Zheng Y. Fourier transform infrared spectroscopy of "Bisphenol A". J Spectrosc. 2016;1:2073613. https://doi.org/10.1155/2016/2073613.
52. Tsai WT, Lai CW, Su TY. Adsorption of bisphenol-A from aqueous solution onto minerals and carbon adsorbents. J Hazard Mater. 2006;134(1-3):169-75. http://doi.org/10.1016/j.jhazmat.2005.10.055. PMid:16343748.
53. Supong A, Bhomick PC, Baruah M, Pongener C, Sinha UB, Sinha D. Adsorptive removal of Bisphenol A by biomass activated carbon and insights into the adsorption mechanism through density functional theory calculations. Sustain Chem Pharm. 2019;13:100159. http://doi.org/10.1016/j.scp.2019.100159.
54. Balarak D. Kinetics, isotherm and thermodynamics studies on bisphenol a adsorption using barley husk. Int J Chemtech Res. 2016;9(5):681-90.
55. Sudhakar P, Mall ID, Srivastava VC. Adsorptive removal of bisphenol-A by rice husk ash and granular activated carbon: A comparative study. Desalination Water Treat. 2016;57(26):12375-84. http://doi.org/10.1080/19443994.2015.1050700.
56. Tran HN, You SJ, Chao HP. Thermodynamic parameters of cadmium adsorption onto orange peel calculated from various methods: a comparison study. J Environ Chem Eng. 2016;4(3):2671-82. http://doi.org/10.1016/j.jece.2016.05.009.
57. Srivastava V, Sharma YC, Sillanpää M. Application of nano-magnesso ferrite (n-MgFe 2 O 4) for the removal of Co 2+ ions from synthetic wastewater: Kinetic, equilibrium and thermodynamic studies. Appl Surf Sci. 2015;338:42-54. http://doi.org/10.1016/j.apsusc.2015.02.072.
58. Akande JA, Adeogun A, Uzosike AS. Removal of congo red dye from simulated wastewater using activated carbon derived from corn cobs; kinetics and equilibrium studies. Glob J Pure Appl Chem Res. 2023;11(1):1-19. http://doi.org/10.37745/gjpacr.2013/vol11n1119.
59. Tang S, Ma S, Zhang T, Liu X, Nahid Pervez M, Cao C, et al. Sorption of bisphenol A onto microplastics and associated environmental risks in comparison to engineered carbonous materials and natural media. Gondwana Res. 2023;117:295-306. http://doi.org/10.1016/j.gr.2023.02.014.
60. Rahmat NA, Hadibarata T, Yuniarto A, Elshikh MS, Syafiuddin A. Isotherm and kinetics studies for the adsorption of bisphenol A from aqueous solution by activated carbon of Musa acuminata. IOP Conf Ser Mater Sci Eng. 2019;495:012059. http://doi.org/10.1088/1757-899X/495/1/012059.

Data Availability

The entire dataset that supports the results of this study has been published within the article itself